Cerebral Cortex, March 2019;29: 1218–1229

doi: 10.1093/cercor/bhy028
Advance Access Publication Date: 7 February 2018
Original Article

ORIGINAL ARTICLE

System-Specific Patterns of Thalamocortical Connectivity in Early Brain Development as Revealed by Structural and Functional MRI

Silvina L. Ferradal[1], Borjan Gagoski[1], Camilo Jaimes[2], Francesca Yi[1], Clarisa Carruthers[1], Catherine Vu[1], Jonathan S. Litt[3], Ryan Larsen[4], Brad Sutton[4], P. Ellen Grant[1] and Lilla Zöllei[2]

[1]Boston Children's Hospital, Harvard Medical School, Boston, MA 02115, USA, [2]Massachusetts General Hospital, Harvard Medical School, Boston, MA 02114, USA, [3]Beth Israel Deaconess Medical Center, Boston, MA 02215, USA and [4]Beckman Institute, University of Illinois at Urbana-Champaign, Urbana, IL 61801, USA

Address correspondence to Silvina L. Ferradal, Fetal-Neonatal Neuroimaging & Developmental Science Center, Boston Children's Hospital, 300 Longwood Avenue, Boston, MA 02215, USA. Email: silvina.ferradal@gmail.com.

Abstract

The normal development of thalamocortical connections plays a critical role in shaping brain connectivity in the prenatal and postnatal periods. Recent studies using advanced magnetic resonance imaging (MRI) techniques in neonates and infants have shown that abnormal thalamocortical connectivity is associated with adverse neurodevelopmental outcomes. However, all these studies have focused on a single neuroimaging modality, overlooking the dynamic relationship between structure and function at this early stage. Here, we study the relationship between structural and functional thalamocortical connectivity patterns derived from healthy full-term infants scanned with diffusion-weighted MRI and resting-state functional MRI within the first weeks of life (mean gestational age = 39.3 ± 1.2 weeks; age at scan = 24.2 ± 7.9 days). Our results show that while there is, in general, good spatial agreement between both MRI modalities, there are regional variations that are system-specific: regions involving primary-sensory cortices exhibit greater structural/functional overlap, whereas higher-order association areas such as temporal and posterior parietal cortices show divergence in spatial patterns of each modality. This variability illustrates the complementarity of both modalities and highlights the importance of multimodal approaches.

Key words: early development, functional connectivity, neonates, probabilistic tractography, thalamus

Introduction

Areal specification of the human cerebral cortex is thought to begin in the ependymal zone where proliferative units lay down a proto-map of the cerebral cortex that is translated to the cortical plate by radial glial guides (Rakic 1988). According to this "Radial Unit" hypothesis, thalamocortical axons play an important role in modulating areal specification (O'Leary et al. 2007; Lokmane et al. 2013; Martini et al. 2018). Thalamocortical afferents start to appear prenatally around the eighth postconceptual week (PCW) and reach the cortical plate by midgestational age (24–25th PCW). Early synapses in the deep layers of the cortical plate are first established by the 26th PCW (Kostovic and Jovanov-Milosevic 2006; Kostovic and Judas 2010), and a few weeks later, thalamic fibers reach their final destination in more superficial layers, establishing synapses mainly at the cortical layer IV (Kostovic and Judas 2010). During the first

months after birth, there is a phase of increasing connectivity which is further refined by selective pruning that lasts until adolescence (Innocenti 1995; Bourgeois 1997). The maturation of thalamocortical connections are reflected by the emergence of somatosensory-evoked potentials (SEP) (Vanhatalo and Lauronen 2006). In the early preterm period, as thalamic afferents enter the cortical plate (24–25th PCW), long and delayed cortical activations can be detected in the deep layers. Faster cortical responses emerge later as the thalamic fibers accumulate synapses in cortical layer IV.

The development of thalamocortical connections during the mid and late gestational periods plays a critical role in shaping brain connectivity during prenatal and early postnatal life (Ghosh et al. 1990; McQuillen and Ferriero 2005; Kostovic and Judas 2010). Recent studies have shown that alterations in thalamocortical connectivity are associated with adverse neurological outcome after immature birth (Ball et al. 2013, 2015; Fischi-Gomez et al. 2015; Thompson et al. 2016) or brain damage due to hypoxic-ischemic insults (de Vries and Jongmans 2010; Dean et al. 2013). This suggests that the thalamus acts as a key hub for cortical networks and that alterations in thalamocortical connectivity may portent aberrant corticocortical connectivity, establishing the thalamocortical system as a clinically relevant target for early detection and assessment of abnormal brain development originating prenatally and/or in the early postnatal period.

Advanced imaging techniques such as diffusion-weighted magnetic resonance imaging (DWI) and resting-state functional MRI (rs-fMRI) have been used to track the structural and functional trajectories in the developing brain. While the majority of these studies have focused on understanding the corticocortical organization in term and preterm infants (Doria et al. 2010; Smyser et al. 2011; Gao et al. 2015), there has been recent interest in exploring the corticosubcortical organization in infants and children (Fair et al. 2010; Alcauter et al. 2014; Greene et al. 2014; Ball et al. 2015; Poh et al. 2015; Toulmin et al. 2015). Using longitudinal rs-fMRI data at birth, 1 and 2 years, Alcauter and colleagues described the developmental changes of thalamocortical functional connectivity (Alcauter et al. 2014). Thalamus-sensorimotor and thalamus-salience networks were identified in neonates, while thalamus-medial visual and thalamus-default mode networks were not evident until 1 year of age. In this study, thalamus-salience connectivity at 1 year was the only thamalocortical network that correlated with behavioral outcomes at 2 years. Toulmin and colleagues used a similar approach in term and prematurely-born infants where they showed that functional connectivity patterns at term are correlated with the degree of prematurity (Toulmin et al. 2015). Using DWI data, Ball et al. (2015) used a complementary approach to show that thalamocortical structural connectivity patters in the preterm brain measured at term equivalent age are correlated with cognitive performance in early childhood. Despite these promising results, all of these prior studies focused on either functional or structural connectivity. As a result, little is known about the complex interplay between the thalamocortical structural and functional connectivity patterns at early postnatal ages.

While function is shaped and constrained by brain structure (Honey et al. 2007, 2009), structure can be modified by functional activity stimulated by environmental inputs (Draganski et al. 2004; Zatorre et al. 2012). At early stages of life, this relationship is particularly dynamic due to maturational processes such as experience-dependent pruning of exuberant connections (O'Leary 1992; Innocenti and Price 2005), consolidation of long-range axonal projections (Kostovic and Jovanov-Milosevic 2006; Takahashi et al. 2012; Thomason et al. 2015) and myelination (Brody et al. 1987; Barkovich et al. 1988); all of which are expected to introduce rapid changes in structural and functional brain connectivity. Insult during this developmentally critical period may promote the recruitment of alternative anatomical pathways to sustain a given function (Uylings 2006), affecting the specification and integration of functional circuits at cortical and subcortical levels. Future studies which combine structural and functional connectivity may therefore lead to a better understanding of neural mechanisms involved in adverse outcomes. However, before such approaches can be used in the infant population, the relationship between structural and functional connectivity in normal infants, beginning with the neonate, must be understood.

In this study, we characterize thalamocortical connectivity patterns in the newborn brain derived from structural (SC) and functional connectivity (FC) analysis and explore the spatial relationships between both modalities. Many technical challenges preclude accurate estimation of connectivity maps in early infancy: lack of age-specific segmentation tools, lack of age-matched brain templates, inaccurate anatomical regions-of-interest (ROIs), motion contamination, etc. Here, we propose an image analysis pipeline customized to address these issues in neonatal populations. We hypothesize that, based on the known early patterns of cortical organization (Lagercrantz et al. 2010) and myelin maturation (Brody et al. 1987; Barkovich et al. 1988), the agreement between structural and functional connectivity maps will be system-dependent, with sensory systems showing stronger overlaps than higher-order cognitive regions.

Materials and Methods

Participants

Healthy, full-term neonates were recruited at the Brigham and Women's Hospital (BWH) and Beth Israel Deaconess Medical Center (BIDMC) as part of an ongoing prospective data collection study. The protocol was reviewed and approved by the institutional review boards at Boston Children's Hospital, BWH and BIDMC. Written consent was obtained from parents. Only full-term neonates whose mothers had no known medical conditions or complications during pregnancy were included in the study. For this particular study, we evaluated a total of 49 datasets and kept the 20 datasets showing the best quality in the MPRAGE, rs-fMRI, and DWI volumes. The reason for discarding a dataset was either due to incomplete data (n = 20), that is, lacking at least one of the 3 sequences, or poor data quality in at least one of the 3 sequences (n = 9). All subjects were full-term infants (gestational age at birth: 39.3 ± 1.2 weeks) scanned within their first month of life (age at scan: 24.2 ± 7.9 days). Additional information regarding age at birth and at time of scan, birthweight, occipital frontal circumference (OFC), sex, and ethnicity is provided in Table 1.

Image Acquisition

Infants were scanned during natural sleep using a Siemens 3T Trio with a 32-channel adult head coil. A motion-compensated multiecho MPRAGE sequence (van der Kouwe et al. 2008; Tisdall et al. 2012) was obtained in the sagittal plane with an image resolution of $1 \times 1 \times 1\,mm^3$. Diffusion-weighted images (TE = 104 ms, TR = 3700 ms, in-plane voxel size = $2 \times 2\,mm^2$,

Table 1 Gestational age (GA) at birth and at time of scan, birthweight, occipital frontal circumference (OFC), sex and ethnicity. GA at birth and at time of scan, as well as birthweight and head circumference are displayed as mean ± standard deviation

GA at birth (weeks)	Range (weeks)	GA at scan (weeks)	Range (weeks)	Birthweight (kg)	OFC (cm)	Male (%)	Caucasian (%)
39.3 ± 1.2	36.4–41.1	42.7 ± 1.8	40.1–46.2	3.4 ± 0.6	33.7 ± 2.1	50	45

slice thickness = 2 mm) were acquired with thirty directions at b = 1000 s/mm^2 and thirty directions at b = 2000 s/mm^2, accelerated with 2 × GRAPPA and simultaneous multislice (SMS) factor of 2. Blood-oxygen level dependent (BOLD) weighted imaging was acquired (TE = 36 ms, TR = 1360 ms, in-plane voxel size = 2 × 2 mm^2, slice thickness = 2 mm) with SMS factor of 3. One resting-state BOLD acquisition of 350 time points (~8 min) was obtained for each infant. Both DWI and resting-state BOLD acquisitions are EPI-based readouts.

ROI Definition

All our manual and automated segmentations were carried out on the MPRAGE scans. Two experts made sure that the input images, acquired with online motion correction, had sufficient contrast for the segmentation task as well as that the resulting ROI labels were accurate. Our prior-based multiatlas label fusion tool relies on a database of 26 manually segmented T1-weighted images for guidance.

Anatomical Masks

After skull-stripping using a modified version of the tool developed by Doshi et al. (2013), automatic subject-specific white matter (WM) and gray matter (GM) masks (Fig. 1*c*) were computed using a prior-based Bayesian approach. The method is a modification to the label fusion algorithm described in Iglesias et al. (2012), where we relied on ground-truth information from a manually annotated training data described by de Macedo Rodrigues et al. (2015). The cerebrospinal fluid (CSF) mask was defined by the difference between the skull-stripped input datasets and the GM label.

Cortical Labels and Thalamus

For all subjects, we obtained an automatic segmentation, on both hemispheres, of the lobar ROIs in the cortical ribbon from the structural MPRAGE scans (Fig. 1*d*). All segmentations were carried out in the native space of each acquisition (without any transformation to a standard analysis space). The set of cortical labels used in this study follows those from the adult connectivity and infant resting-state literature (Fair et al. 2010): prefrontal cortex, premotor cortex, primary motor cortex, somatosensory cortex, posterior parietal cortex, occipital cortex, and temporal cortex. In order to define and identify their location, we used journal paper descriptions of adult studies, anatomy references and the FreeSurfer adult brain segmentation descriptions (Fischl et al. 2002, 2004; Johansen-Berg et al. 2005; Desikan et al. 2006; Ratiu and Talos 2006; Despotovic et al. 2010). Due to limited spatial resolution, sulcal delineation in the volumetric space is a challenge. With our structural image resolution of 1 mm^3, 2 adjacent cortical areas and the interposed sulcus often shared the same voxel. Therefore, for the tractography analysis, we slightly shifted the boundaries of our target regions towards the WM when partial voluming was too severe to allow us to draw them strictly in the GM (Fig. 1*e*). Placing the target areas in the juxtacortical WM also increased the chances of successful tracking outcome to that specific area as opposed to a target located entirely in the cortex. These refinements were manually performed using FreeView (FreeView) by either an experienced neuroradiologist (C.J.) or a specifically trained research assistant (F.Y.). To maintain accuracy and consistency, the resulting segmentations of all subjects were reviewed, corrected, and finalized by the same neuroradiologist (C.J.) in the 3 orthogonal planes for tridimensional accuracy check.

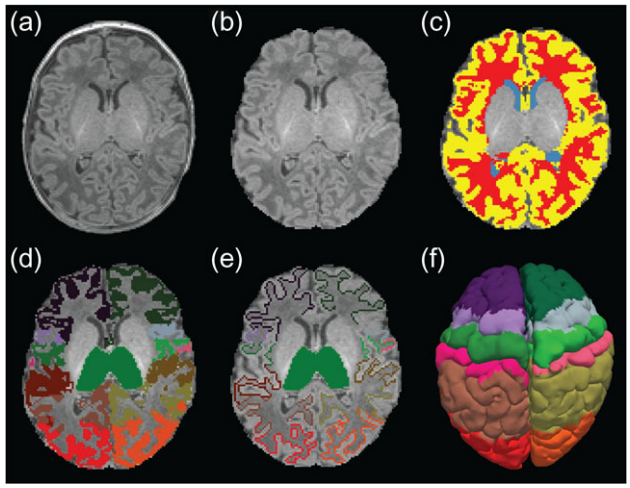

Figure 1. Anatomical images of a single subject and its corresponding segmentations in native space. (*a*) Original T1-weighed MRI, (*b*) brain extracted MRI, (*c*) automatically generated anatomical masks: CSF (blue), WM (red), GM (yellow), and thalamic and cortical labels used for (*d*) functional connectivity and (*e*) probabilistic tractography analysis. (*f*) Pial cortical surface showing cortical regions used for connectivity analysis (following FreeSurfer standard color lookup table).

In addition to the cortical regions, the left and right thalamus were also manually identified (Fig. 1*d*,*e*). We defined the boundaries of these major central GM nuclei by the body of the lateral ventricles and the transverse fissure superiorly and medially, by the ventral diencephalon and mesencephalon inferiorly, by the third ventricle inferiorly and medially, and by the hippocampus and crus of the fornices posteriorly. Access to such segmentation labels facilitated importing anatomically meaningful regions of interest into the connectivity-based parcellation that correspond to the areas analyzed in adult studies (Johansen-Berg et al. 2005).

Neonatal Template for Group Comparisons

A neonatal spatial reference space was created for computing our group connectivity maps and visualizing our results. In total, 43 MPRAGE input MRI volumes—collected as part of the above described study, but not part of the cohort included in the current connectivity analysis as subjects either lacked good rs-fMRI or DWI volumes—were registered in a statistically unbiased manner, weighing all input images equally, using the affine version of the image registration framework described in Reuter et al. (2012).

Image Analysis

The complete processing pipeline is summarized in Supplementary Figure S1.

rs-fMRI Preprocessing

We used FSL tools and in-house scripts for preprocessing the resting-state BOLD data. Preprocessing steps included: (1) slice timing correction for SMS BOLD acquisitions, (2) head motion correction within and across runs, (3) estimation of motion regressors, and (4) intensity normalization (after removing the first 4 frames of each BOLD run to allow for stabilization of the magnetic field). Individual functional connectivity analysis was performed in the native functional space so subject-specific anatomical masks were mapped to this space using a rigid transformation (FSL/flirt) (Jenkinson et al. 2002) computed between each individual MPRAGE scan and the first frame of the realigned BOLD sequence. Linear regression was performed using the following nuisance regressors: (1) 6 motion regressors from realignment estimates (accounting for translations and rotations in 3 directions), and (2) mean CSF and WM signals extracted from the subject-specific anatomical masks. In order to remove physiological contamination such as heart rate, temporal band-pass filtering (0.008–0.09 Hz) was applied to the demeaned and detrended BOLD time-series after linear regression and scrubbing. Global signal regression was not performed as part of the functional connectivity analysis. Instead, we opted for partial correlation analysis between each thalamic voxel and cortical ROI, which computes the correlation only after eliminating any globally shared signals (Birn et al. 2006). Spatial smoothing was then applied using a Gaussian filter with a full width at half maximum (FWHM) of 4 mm.

Scrubbing and Interpolation of Corrupted rs-fMRI Data

Before temporal filtering and spatial smoothing, frames corrupted by motion were excluded from further analysis using an established motion detection strategy (Smyser et al. 2010; Power et al. 2012). Motion metrics considered frame-by-frame displacements (FD) derived from the realignment estimates from motion correction as well as frame-by-frame signal intensity changes (DVARS) computed as the root-mean-squared BOLD signal intensity change after preprocessing. Frames with FD > 0.25 mm and DVARS > 3 were removed from the BOLD time-series. In order to minimize potential artifacts in neighboring volumes due to temporal filtering or spin history, 2 frames before and after the censored volumes were also removed. To avoid the potential introduction of edge effects due to temporal filtering, the corrupted frames were replaced using *b*-spline interpolation. The interpolated frames were not considered in the partial correlation analysis. A minimum of 5 min of usable rs-fMRI data were required for inclusion in subsequent analyses. The mean number of frames used across subjects after scrubbing was 305 (~6.9 min), while the mean FD and DVARS were 0.066 mm and 1.19, respectively. Supplementary Figure S2 shows the percentage of rs-fMRI frames kept after scrubbing.

Functional Connectivity Analysis

Subject-specific masks for thalamic and cortical regions were mapped to the native functional space (see rs-fMRI Preprocessing) and a mean cortical signal was computed for each cortical region. Partial correlations were then computed between the mean cortical signals and the time-series extracted from each thalamic voxel. It is expected that these maps will reflect the individual interactions between each individual cortical region and the thalamus. Partial correlation maps were converted to a normal distribution by Fisher's z-transformation (Jenkins and Watts 1968), registered to a neonatal template (see Neonatal Template for Group Comparisons) and averaged across subjects using a fixed effects model. Group connectivity maps were corrected for multiple comparisons using false discovery rate of 1% ($P = 0.01$).

Quality Control of DWI Data

Signal dropout is the most common artifact observed in the DWI data. Before running the DWI preprocessing steps, a semi-automated KL-divergence-based tool called SignalDropQCTool (Carquex 2015) was used to detect significant dropout values. This tool automatically labels a high *b*-value volume as "bad" if at least one of its slices is affected and "good" if no dropout is detected. Additionally, the "unsure" label is used for volumes with high classification uncertainty. These are the volumes that the tool operator must provide decisions about. Supplementary Figure S2 shows the percentage of DWI volumes kept after quality control (QC) analysis.

DWI Preprocessing

We used tools from the FSL libraries for preprocessing the DWI data (Woolrich et al. 2009). The rigid registration between the MPRAGE and DWI scans acquired on the same subject was carried out by FSL/flirt (Jenkinson et al. 2002) using mutual information as a cost function. All of the resulting transformations were visually inspected for accuracy. In detail, the following steps were performed to obtain connectivity information for each voxel in the examined thalami: (1) extraction of diffusion gradients and the corresponding *b*-values from the input DICOM images, (2) eddy current correction, (3) preprocessing for probabilistic tractography (FSL/bedpostX) (Smith et al. 2004), and (4) probabilistic tractography (FSL/probtrackX) between a predetermined seed region of interest and a list of target ROIs. Note that not all of our images were acquired in a way that FSL/topup (Andersson et al. 2003) and FSL/eddy (Sotiropoulos et al. 2013) could be used with them, thus these tools were not used for this study. However, we selected datasets that exhibited minimal distortion and did not require further preprocessing. To quantify head motion in each scan, we derived volume-by-volume translation and rotation from step (2), as well as slice-by-slice signal dropout measures that are specific to DWI data (Benner et al. 2011). The registration-based measures are better at capturing slower, between-volume motion, whereas the intensity-based measures are better at capturing more rapid, within-volume motion. Tractography then was performed to all cortical targets simultaneously, where probabilistic streamlines terminated once they reached a target region. As described in ROI Definition, the seed ROIs used are the left and the right thalamus and the target ROIs are a set of cortical lobular parcellation labels. The output of the above described probabilistic tractography is a connectivity matrix of size M×N for each subject, where, M indicates the number of targets, that is, 7, and N is the number of voxels in the seed ROI (different for each subject).

Structural Connectivity Analysis

The probability of structural connectivity was computed as the proportion of tracts that propagated from a particular thalamic voxel to a given target ROI. Individual probability maps for each subject were registered to our neonatal template and averaged

across subjects using a fixed effects model. Group probability maps were corrected for multiple comparisons using false discovery rate of 1% ($P = 0.01$).

Quantitative Comparisons Between Structural and Functional Connectivity Patterns

Two different metrics were computed to evaluate the spatial overlap between modalities, namely, the overlap percentage and the Dice coefficient. The overlap percentage was calculated as the fraction of significant voxels in a connectivity map corresponding in space with the significant voxels in the connectivity map of the other modality. The Dice coefficient was calculated as twice the ratio of the overlapping voxels between two connectivity maps to the total number of voxels.

Results

Resting-state fMRI and DWI volumes were obtained in 20 full-term newborn infants scanned during natural sleep within their first month of life (median age at scan: 24 days). The average percentage of rs-fMRI volumes kept after scrubbing is 87.2% while the average percentage of DWI volumes that passed QC is 90.1% (Supplementary Fig. S2). Seven thalamocortical connectivity maps were obtained for each modality based on thalamic and cortical labels segmented from each subject's T1-weighted image. To isolate the functional interactions between thalamus and each cortical region, functional connectivity maps were obtained from partial correlation analysis between the average BOLD signal extracted from the thalamic labels and each individual cortical label (Fig. 2*a*, Supplementary Fig. S3). Structural connectivity maps were derived from the proportion of tracts propagated from thalamic labels on each hemisphere to the ipsilateral cortical labels (Fig. 2*b*, Supplementary Fig. S3). To facilitate spatial comparisons between modalities (Fig. 2*c*), each functional and structural connectivity map was thresholded to 50% of its corresponding 99th percentile value to avoid potential outliers.

Connectivity Maps and Intermodality Comparisons

Group maps derived from functional connectivity analysis (Fig. 2*a*) show a cluster in the anterior and medial aspect of the thalamus corresponding to the prefrontal label, a relatively widespread cluster located in the medial and central thalamus corresponding to the premotor label, and a focal cluster in the lateral aspect of the thalamus corresponding to the primary motor label. A large cluster involving the posterolateral and posteromedial thalamus with extension into the midcentral thalamus is associated to the primary somatosensory label. A very small focal cluster is present along the posterior thalamus corresponding to the posterior parietal label, and a focal cluster along the posteroinferior and medial thalamus corresponds to the occipital label. Finally, a focal cluster in the posteroinferior and lateral thalamus is associated to the temporal label.

Structural connectivity patterns show strong similarities with the FC maps derived for the prefrontal, premotor, primary motor, and occipital labels (Fig. 2*b*). There is a SC cluster in the mediodorsal and anterior thalamus corresponding to the prefrontal label, which is slightly more laterally located than the analogous FC cluster. A SC cluster corresponding to the premotor label extends along the anterior aspect of the ventrolateral thalamus, which is more focal and located more posteriorly and laterally than the analogous FC cluster, while a SC cluster along the ventral aspect of the lateral thalamus corresponding to the primary motor label is located slightly more anteriorly than the analogous FC cluster. There is a focal cluster along the posterior ventrolateral thalamus corresponding to the primary somatosensory label, which is much smaller than the analogous FC cluster. The area of overlap is located along the posterolateral aspect of the larger FC cluster and encompasses the majority of the SC cluster. The SC cluster for the posterior parietal label is located along the posterolateral and posterior thalamus and shows no significant overlap with the small FC cluster. Another SC cluster along the posterior thalamus corresponding to the occipital label is located slightly more anteriorly than the analogous FC cluster. Finally, the cluster for the temporal label is located in the posterior thalamus slightly

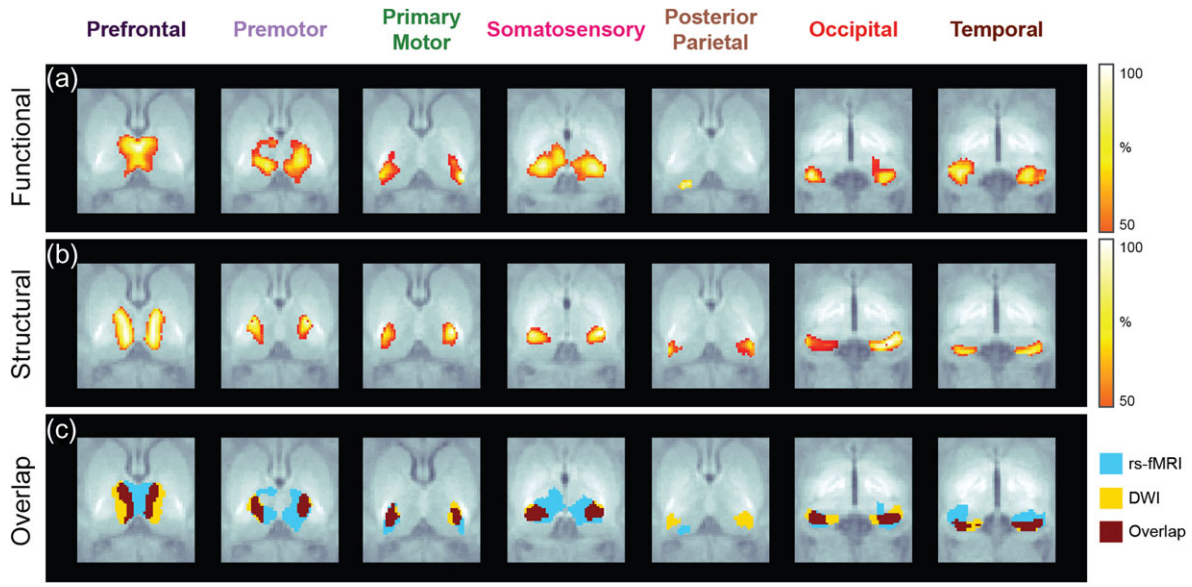

Figure 2. Functional (*a*) and structural (*b*) connectivity maps obtained in a group of 20 healthy neonates. Spatial overlap (*c*) between modalities shows different degrees of spatial agreement.

Table 2 Anatomical location of each functional and structural cluster in the thalamus associated to the 7 cortical regions shown in Figure 2

	Anatomical location of thalamic cluster	
Cortical ROI	Functional	Structural
Prefrontal	Anterior and medial thalamus	Anterior and mediodorsal thalamus
Premotor	Medial and central thalamus	Anterior aspect of the ventrolateral thalamus
Primary motor	Lateral aspect of the thalamus	Ventral aspect of the lateral thalamus
Somatosensory	Posterolateral and posteromedial thalamus with extension into the midcentral thalamus	Posterior ventrolateral thalamus
Posterior parietal	Posterior thalamus	Posterolateral and posterior thalamus
Occipital	Posteroinferior and medial thalamus	Posterior thalamus
Temporal	Posteroinferior and lateral thalamus	Posterior thalamus

Table 3 Spatial overlap between functional and structural connectivity maps. Quantitative comparisons were computed on the thresholded maps shown in Figure 2

Cortical ROI	Overlap percentage	Dice coefficient
Prefrontal	45.2	0.38
Premotor	75.4	0.38
Primary motor	38.3	0.39
Somatosensory	74.0	0.30
Posterior parietal	0	0
Occipital	52.2	0.43
Temporal	38.8	0.29

more posterior than the analogous FC cluster. All these results are summarized in Table 2.

Quantitative intermodality comparisons based on overlap percentage and Dice coefficient show similar results (Table 3). Overall, thalamic regions connected to motor and primary sensory areas exhibit higher overlap percentages and Dice coefficients than regions connected to temporal and posterior parietal cortices. It is worthwhile to mention that the discrepancy between overlap percentage and Dice coefficient in the premotor and somatosensory cortices is likely due to differences in the size of the clusters measured with each modality. While both metrics are sensitive to the relative locations of the FC/SC clusters, the Dice coefficient is also sensitive to their relative sizes. This means that if a smaller cluster is mostly contained within a larger one, the Dice coefficient will be smaller. For example, the SC cluster for the somatosensory label is contained within the larger FC cluster. Consequently, despite a very high overlap percentage, the Dice coefficient is lower than that of other clusters with high overlap percentages such as the prefrontal clusters.

Thalamic Parcellations

A winner-takes-all strategy provided an alternative approach to summarize the individual connectivity maps into a single thalamic parcellation map (Fig. 3), where cortical labels were assigned to each thalamic voxel based on the highest partial correlation or probability value.

As already mentioned by Toulmin et al. (2015), it is not possible to identify thalamic nuclei from individual structural MR images as the neonatal thalamus does not have sufficient intrinsic T1 or T2 contrast. Given the lack of atlases of thalamic histology for neonatal populations, the best anatomical reference can be provided by adult atlases. However, direct anatomical registration of neonatal images to adult templates may compromise the accuracy in identifying the neonatal anatomy, particularly in small structures such as the thalamus, due to significant developmental changes occurring during this period. Thus, henceforth, we only suggest potential alignments between the functional and structural thalamic clusters obtained from the neonatal parcellation maps and the adult thalamic nuclei identified by histology (Mai et al. 2007).

The functional parcellation map shows a predominant thalamic cluster associated to the primary somatosensory cortex. In comparing with adult histology, this cluster extends along the expected location of the ventral posterior–lateral and lateral posterior nuclei. In addition, it seems to extend beyond the expected boundaries of the somatosensory clusters involving parts of the ventral lateral and possibly the ventral anterior nuclei (Fig. 3*b*). There are 2 smaller clusters associated to the premotor and primary motor cortices which potentially extend along the ventral anterior and ventral lateral nuclei, respectively. Another significantly large cluster associated to the prefrontal cortex extends along the presumed location of the mediodorsal and anterior nuclei and probably the ventral anterior nucleus, while the temporal cortex presents a cluster located along the pulvinar nucleus. Finally, a small cluster associated to the occipital cortex is located in the expected location of the lateral geniculate nucleus. No cluster associated with the posterior parietal cortex was observed in the functional thalamic parcellation map, consistent with the results reported by Toulmin et al. (2015).

The structural parcellation map exhibits a cluster associated to the prefrontal cortex which is potentially aligned with the medial and ventral anterior nuclei (Fig. 3*c*). Consistent with the clusters obtained from the functional parcellation, there are 2 structural clusters associated to the premotor and primary motor cortices that extend along the lateral surface of the thalamus in the expected location of the ventral anterior and ventral lateral nuclei, respectively. The temporal cortex has a thalamic cluster that extends along the pulvinar nucleus, consistent with the analogous functional cluster. By contrast with the functional results, the posterior parietal cortex exhibits a structural cluster than extends along the ventral posterior nucleus. Interestingly, the structural cluster associated to the primary somatosensory cortex is very focal and small.

The parcellation maps only show dominant connectivity and disregard the contribution of multiple cortical regions on each thalamic voxel, ignoring the integrative nature of the thalamic circuits. Figure 4 shows the number of cortical regions significantly ($P < 0.01$) connected to each thalamic voxel for both modalities. The midthalamic voxels in the functional maps show significant connections with 3–4 cortical regions

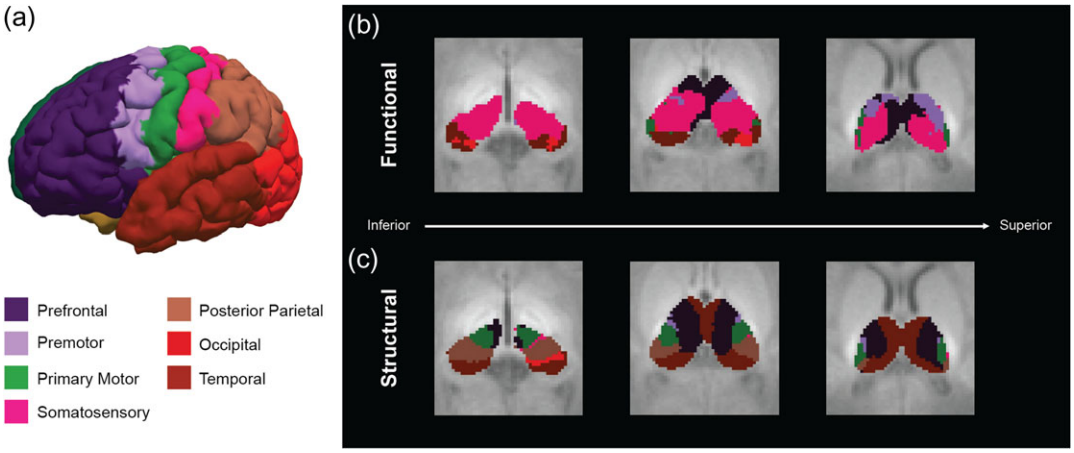

Figure 3. Thalamic parcellations. (*a*) Cortical surface showing the 7 cortical regions used in the connectivity analysis. Functional (*b*) and structural (*c*) thalamic parcellations were color-coded based on the FreeSurfer standard color lookup table.

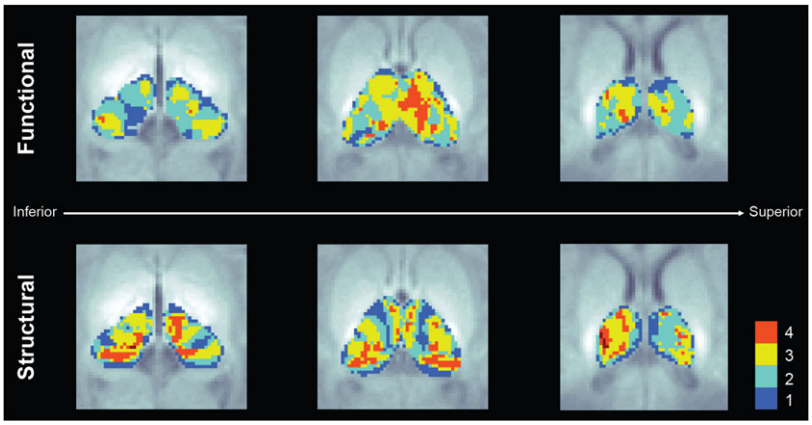

Figure 4. Number of cortical regions with significant thalamocortical connectivity derived from the functional (top) and structural (bottom) connectivity analysis.

(prefrontal, premotor, primary motor, and somatosensory), while the lateral areas show connections with only 2 or 1 cortical label. In the case of the structural maps, a slightly different pattern is observed, with thalamic voxels located in midcentral and posterior areas connected to 3–4 cortical labels (prefrontal, premotor, primary motor, and temporal) and with thalamic voxels in the lateral areas connected to 1–4 cortical labels (premotor, primarily motor, somatosensory, and posterior parietal).

Discussion

This study presents, to our knowledge, the first combined analysis of the structural and functional thalamocortical connectivity patterns in the newborn brain. Prior reports comparing both MRI modalities focused exclusively on the adult brain (Zhang et al. 2010; Mastropasqua et al. 2015), while studies involving the neonatal brain focused only on a single MRI modality, that is, structural (Poh et al. 2015) or functional connectivity (Alcauter et al. 2014; Toulmin et al. 2015). Overall, we show robust bilateral connectivity maps in both modalities that resemble the structural (Behrens, Johansen-Berg, et al. 2003; Johansen-Berg et al. 2005) and functional (Zhang et al. 2008; Fair et al. 2010) topographies observed in healthy adults, suggesting that relatively mature thalamocortical circuits can be detected at the time of birth. Despite the general agreement with the adult thalamic structural organization (Zhang et al. 2010), there are regional variations in the SC/FC spatial relationship that presumably reflect differential rates of maturation. The current analysis shows that thalamic regions connected to motor and primary sensory cortices (i.e., occipital and somatosensory) exhibit greater spatial overlap than regions connected to higher-order association areas such as temporal and posterior parietal cortices.

Our analysis methods were customized specifically for neonatal populations with the goal of producing accurate results: anatomical labels were automatically created based on subject-specific structural images, an age-matched neonatal atlas extracted from the same population was used for group comparisons and stringent motion correction criteria was applied to the functional and structural data, preserving only volumes with minimal motion (mean FD < 0.07 mm and mean DVARS < 1.2 after scrubbing rs-fMRI data; average translation = 1.04 mm, average rotation = 0.013 radians after QC of DWI data). Also, since the rs-fMRI and DWI scans were performed on the same cohort, the influence of interindividual variability was minimized between modalities.

While it is generally assumed that the functional connectivity patterns are reflective of the underlying anatomical connections (Honey et al. 2009), the development of SC and FC networks in the early postnatal brain is significantly influenced

by the heterogeneous patterns of maturation conceivably dominated by myelination (Brody et al. 1987; Barkovich et al. 1988), axonal pruning (Rakic and Riley 1983; LaMantia and Rakic 1990; Petanjek et al. 2011) and synaptic development (Huttenlocher et al. 1982; Montgomery and Madison 2004). As held by Yakovlev and Lecours (1967), myelination represents the anatomic correlate of neurophysiological maturation. Our thalamocortical connectivity maps seem to be consistent with prior studies showing that myelination maturation proceeds along a hierarchy of increasingly complex functional processing, with sensory pathways myelinating first, followed by motor pathways and finally ending in the maturation of association and intracortical fibers critical for cognitive processing (Barkovich et al. 1988; Huttenlocher 2002).

It is widely accepted that these structural processes are initially shaped by early spontaneous neuronal activity and, later in development, refined by stimulus-driven, activity-dependent mechanisms (Shatz 1996; Dehaene and Changeux 2005). As shown by Vanhatalo and Lauronen (2006), the maturation of thalamocortical connections is intrinsically related to cycles of endogenous neuronal activity during the midprenatal period which is followed by synchronized brain activity during the late prenatal period, marking the emergence of synchronized functional networks (Lagercrantz et al. 2010). In effect, fMRI studies performed in late preterm and full-term neonates (Doria et al. 2010; Smyser et al. 2010; Fransson et al. 2011; Gao et al. 2015) have shown relatively well developed functional networks in motor and primary sensory cortices (e.g., visual system) at birth. This is consistent with reports suggesting that neonates already display a basic level of consciousness through sensory awareness especially to painful stimuli, maternal speech and odors (Lagercrantz et al. 2010).

The presence of robust thalamocortical circuits involving primary sensory and salience processing—the latter represented by thalamic connectivity to the prefrontal cortex, comprising the anterior cingulate cortex and anterior insula, and located in the dorsomedial nucleus of the thalamus (Seeley et al. 2007)—is consistent with the notion that the basic functional circuits essential for survival are already established at birth. In particular, the anterior insula has connections with limbic structures involved in affective processing (Uddin 2015) as well as olfactory, gustatory and viscero-autonomic functions (Afif et al. 2007). Since the insular cortex is a structure that emerges early in life—around the sixth PCW—it is not surprising that we observe thalamocortical circuits involving the salience network at the time of birth. Our functional connectivity patterns are consistent with previous results reported by Alcauter et al. (2014) and our structural connectivity maps extend them to their structural counterparts.

The differences between SC and FC maps are most striking if we compare the thalamocortical parcellations defined by the regions with the highest probability/connectivity at each thalamic voxel. The spatial topology of the structural parcellations show a good resemblance to thalamic parcellations observed in adults (Zhang et al. 2010), indicating that the structural substrates of the adult-like thalamic organization are already established at birth. By contrast, the functional parcellations are markedly weighted towards primary sensory areas, concurrent with functional studies showing that cortical hubs at this early age are dominated by processes related to perception–action behavior, typically associated with sensorimotor, primary auditory and visual networks (Fransson et al. 2011; Gao et al. 2011). Previous investigations have shown that as maturation progresses, these lower-order cortical hubs gradually decrease in importance relative to hubs located in higher-order association areas typically found in adults and adolescents (Fair et al. 2009; Hwang et al. 2013; Grayson et al. 2014). It is expected that the development of thalamic organization is synchronized with cortical maturation and thus, as a result of this functional reorganization, the overlap between both modalities will progressively increase with age. In fact, several studies have shown that the association between FC and SC is remarkably significant in healthy young adults (Hagmann et al. 2008; Skudlarski et al. 2008; Damoiseaux and Greicius 2009), while this relationship is immature in children (Fair et al. 2008; Supekar et al. 2010). Interestingly, studies of aging show decreasing convergence of SC and FC (Fjell et al. 2017; Tsang et al. 2017) suggesting that maturation and aging may drive correlations in different directions. Further investigations to understand the biological mechanisms of these changes in longitudinal studies are needed.

The overlap of SC and FC parcellations show striking regional differences particularly in the primary somatosensory and posterior parietal labels. The FC cluster for the primary somatosensory label was the largest of all the FC clusters and was located in the posterolateral, posteromedial, and midcentral thalamus, extending beyond the expected anatomic boundaries of the ventral posterior nucleus, the primary thalamic sensory nucleus. This is consistent with the results first reported by Alcauter et al. (2014), which also showed the neonatal thalamus to be dominated by the sensorimotor FC cluster. The extension into the posteromedial and midcentral thalamus potentially overlaps with the expected anatomic location of additional nuclei and nuclear groups including the pulvinar, lateral posterior, lateral dorsal, ventral lateral, and medial nuclei, that are involved in a variety of sensory, motor, and cognitive tasks (Nieuwenhuys et al. 2008). By contrast, the posterior parietal label has only a small cluster in the posterior thalamus, which shows no significant overlap with the analogous SC cluster. These observations are consistent with the results from Toulmin et al. (2015), which showed that the primary sensorimotor cortex had widespread FC in the thalamus. Similar to these authors, we hypothesize that the overlap in topographic organization in the thalamus could be due to the more advanced functional integration properties of the sensorimotor cortices at term age. Intrathalamic connectivity circuits are known to exist (Crabtree and Isaac 2002) and could provide polysynaptic functional integration of the neonatal sensorimotor cortex, giving rise to the large thalamic region on the rs-fMRI maps. We also hypothesize that the lack of overlap in structural and functional thalamic connections to posterior parietal regions may indicate less advanced functional integration of this region at term age due its known delayed maturation compared with sensorimotor regions (Huttenlocher and Dabholkar 1997; Counsell et al. 2002; Travis et al. 2005). Therefore, not only the maturation of corticothalamic connections but also the maturation of intrathalamic modulatory systems are likely to play a significant role in thalamocortical resting-state functional connectivity.

Conversely, we hypothesize that the more restricted structural connectivity of the thalamus to sensorimotor cortex, may represent the monosynaptic segregation of thalamic connectivity to the expected location of the VL/VPL thalamus. For the estimation of structural connectivity, we used probabilistic tractography instead of streamline methods because it is more reliable at characterizing crossing fibers (Behrens, Woolrich, et al. 2003). However, we cannot rule out the possibility that less likely connections might be overpowered by the larger

ones, particularly at this early age where exuberant connectivity is expected. Thus, the tractography results, although optimized to retain crossing fibers, are likely an underestimate of existing axonal connections and likely represent the most coherent ones, retaining only direct structural connections between the thalamus and cortex.

This study is limited by the inability to resolve individual thalamic nuclei on anatomical scans (Toulmin et al. 2015). As a result, we cannot confirm the accuracy of the partitions provided by our diffusion approach or confirm the nuclei involved in the rs-fMRI partitions. We can only make suggestions based on histological identification of thalamic nuclei in adults (Mai et al. 2007). In addition, although we probe tissue structure at the micron level with DTI, a 2 mm voxel size results in significant averaging over orders of magnitude and therefore insensitivity to incoherent microstructure (Xu et al. 2014). Our rs-fMRI also suffers from volume averaging given the same 2 mm voxel size which results in an inability to distinguish the reticular nucleus, a key regulatory nuclei in the thalamus (Lam and Sherman 2011). Finally, our rs-fMRI analysis assumes mature neurovascular coupling and correlates changes in regional deoxyhemoglobin change instead of regional oxygen consumption. This may result in misleading findings as the etiology of slow hemodynamic activity in neonates is unknown and regional oxygen consumption is likely to be more accurate (Kozberg and Hillman 2016).

Conclusions

A better understanding of the relationship between functional maturation and the evolving structural organization in early development is crucial to evaluate how alterations in functional and structural connectivity can occur as a consequence of neurological injuries. This study provides a characterization of this relationship in the first weeks of life using neuroimaging data. The differences observed between SC and FC maps illustrates the complementarity of both modalities and highlights the importance of multimodal approaches. Future investigations should focus on longitudinal approaches that would allow us to track the progression of the SC/FC relationship as a function of maturation.

Supplementary Material

Supplementary material is available at *Cerebral Cortex* online.

Funding

Grant from Abbott Nutrition through the Center for Nutrition, Learning and Memory at the University of Illinois, and NIH grants (R21-HD072505 to P.E.G.), (R01-HD076258 to P.E.G.), and (R00-HD061485-03 to L.Z.). This trial was registered at clinicaltrials.gov as NCT02058225.

Notes

We are grateful to the families for their participation in the study. We thank Lucy Schlink, Naira Link and Erikson Hoff for assisting with the segmentations. We are very grateful to Dr Albert Galaburda for useful discussions and insights on the thalamus' structure and function. We would also like to thank Dr Bruce Fischl for his comments on the manuscript. *Conflict of Interest*: None declared.

References

Afif A, Bouvier R, Buenerd A, Trouillas J, Mertens P. 2007. Development of the human fetal insular cortex: study of the gyration from 13 to 28 gestational weeks. Brain Struct Funct. 212:335–346.

Alcauter S, Lin W, Smith JK, Short SJ, Goldman BD, Reznick JS, Gilmore JH, Gao W. 2014. Development of thalamocortical connectivity during infancy and its cognitive correlations. J Neurosci. 34:9067–9075.

Andersson JL, Skare S, Ashburner J. 2003. How to correct susceptibility distortions in spin-echo echo-planar images: application to diffusion tensor imaging. Neuroimage. 20: 870–888.

Ball G, Boardman JP, Aljabar P, Pandit A, Arichi T, Merchant N, Rueckert D, Edwards AD, Counsell SJ. 2013. The influence of preterm birth on the developing thalamocortical connectome. Cortex. 49:1711–1721.

Ball G, Pazderova L, Chew A, Tusor N, Merchant N, Arichi T, Allsop JM, Cowan FM, Edwards AD, Counsell SJ. 2015. Thalamocortical connectivity predicts cognition in children born preterm. Cereb Cortex. 25:4310–4318.

Barkovich AJ, Kjos BO, Jackson DE Jr., Norman D. 1988. Normal maturation of the neonatal and infant brain: MR imaging at 1.5 T. Radiology. 166:173–180.

Behrens TE, Johansen-Berg H, Woolrich MW, Smith SM, Wheeler-Kingshott CA, Boulby PA, Barker GJ, Sillery EL, Sheehan K, Ciccarelli O, et al. 2003. Non-invasive mapping of connections between human thalamus and cortex using diffusion imaging. Nat Neurosci. 6:750–757.

Behrens TE, Woolrich MW, Jenkinson M, Johansen-Berg H, Nunes RG, Clare S, Matthews PM, Brady JM, Smith SM. 2003. Characterization and propagation of uncertainty in diffusion-weighted MR imaging. Magn Reson Med. 50: 1077–1088.

Benner T, van der Kouwe AJ, Sorensen AG. 2011. Diffusion imaging with prospective motion correction and reacquisition. Magn Reson Med. 66:154–167.

Birn RM, Diamond JB, Smith MA, Bandettini PA. 2006. Separating respiratory-variation-related fluctuations from neuronal-activity-related fluctuations in fMRI. Neuroimage. 31:1536–1548.

Bourgeois JP. 1997. Synaptogenesis, heterochrony and epigenesis in the mammalian neocortex. Acta Paediatr Suppl. 422: 27–33.

Brody BA, Kinney HC, Kloman AS, Gilles FH. 1987. Sequence of central nervous system myelination in human infancy. I. An autopsy study of myelination. J Neuropathol Exp Neurol. 46: 283–301.

Carquex C. 2015. Quality control in diffusion weighted MRI [Masters]. Lyon, France: National Institute of Applied Sciences.

Counsell SJ, Maalouf EF, Fletcher AM, Duggan P, Battin M, Lewis HJ, Herlihy AH, Edwards AD, Bydder GM, Rutherford MA. 2002. MR imaging assessment of myelination in the very preterm brain. AJNR Am J Neuroradiol. 23:872–881.

Crabtree JW, Isaac JT. 2002. New intrathalamic pathways allowing modality-related and cross-modality switching in the dorsal thalamus. J Neurosci. 22:8754–8761.

Damoiseaux JS, Greicius MD. 2009. Greater than the sum of its parts: a review of studies combining structural connectivity and resting-state functional connectivity. Brain Struct Funct. 213:525–533.

de Macedo Rodrigues K, Ben-Avi E, Sliva DD, Choe MS, Drottar M, Wang R, Fischl B, Grant PE, Zollei L. 2015. A FreeSurfer-compliant

consistent manual segmentation of infant brains spanning the 0–2 year age range. Front Hum Neurosci. 9:21.
de Vries LS, Jongmans MJ. 2010. Long-term outcome after neonatal hypoxic-ischaemic encephalopathy. Arch Dis Child Fetal Neonatal Ed. 95:F220–F224.
Dean JM, McClendon E, Hansen K, Azimi-Zonooz A, Chen K, Riddle A, Gong X, Sharifnia E, Hagen M, Ahmad T, et al. 2013. Prenatal cerebral ischemia disrupts MRI-defined cortical microstructure through disturbances in neuronal arborization. Sci Transl Med. 5:168ra167.
Dehaene S, Changeux JP. 2005. Ongoing spontaneous activity controls access to consciousness: a neuronal model for inattentional blindness. PLoS Biol. 3:e141.
Desikan RS, Segonne F, Fischl B, Quinn BT, Dickerson BC, Blacker D, Buckner RL, Dale AM, Maguire RP, Hyman BT, et al. 2006. An automated labeling system for subdividing the human cerebral cortex on MRI scans into gyral based regions of interest. NeuroImage. 31:968–980.
Despotovic I, Vansteenkiste E, Philips W 2010. Brain volume segmentation in newborn infants using multi-modal MRI with a low inter-slice resolution. Conference Proceedings: Annual International Conference of the IEEE Engineering in Medicine and Biology Society IEEE Engineering in Medicine and Biology Society Conference 2010: pp. 5038–5041.
Doria V, Beckmann CF, Arichi T, Merchant N, Groppo M, Turkheimer FE, Counsell SJ, Murgasova M, Aljabar P, Nunes RG, et al. 2010. Emergence of resting state networks in the preterm human brain. Proc Natl Acad Sci USA. 107: 20015–20020.
Doshi J, Erus G, Ou Y, Gaonkar B, Davatzikos C. 2013. Multi-atlas skull-stripping. Acad Radiol. 20:1566–1576.
Draganski B, Gaser C, Busch V, Schuierer G, Bogdahn U, May A. 2004. Neuroplasticity: changes in grey matter induced by training. Nature. 427:311–312.
Fair DA, Bathula D, Mills KL, Costa Dias TG, Blythe MS, Zhang D, Snyder AZ, Raichle ME, Stevens AA, Nigg JT, et al. 2010. Maturing thalamocortical functional connectivity across development. Front Syst Neurosci. 4:1–10.
Fair DA, Cohen AL, Dosenbach NU, Church JA, Miezin FM, Barch DM, Raichle ME, Petersen SE, Schlaggar BL. 2008. The maturing architecture of the brain's default network. Proc Natl Acad Sci USA. 105:4028–4032.
Fair DA, Cohen AL, Power JD, Dosenbach NU, Church JA, Miezin FM, Schlaggar BL, Petersen SE. 2009. Functional brain networks develop from a "local to distributed" organization. PLoS Comput Biol. 5:e1000381.
Fischi-Gomez E, Vasung L, Meskaldji DE, Lazeyras F, Borradori-Tolsa C, Hagmann P, Barisnikov K, Thiran JP, Huppi PS. 2015. Structural brain connectivity in school-age preterm infants provides evidence for impaired networks relevant for higher order cognitive skills and social cognition. Cereb Cortex. 25: 2793–2805.
Fischl B, Salat DH, Busa E, Albert M, Dieterich M, Haselgrove C, van der Kouwe AJW, Killiany RJ, Kennedy D, Klaveness S, et al. 2002. Whole brain segmentation: automated labeling of neuroanatomical structures in the human brain. Neuron. 33:341–355.
Fischl B, van der Kouwe AJW, Destrieux C, Halgren E, Segonne F, Salat DH, Busa E, Seidman L, Goldstein J, Kennedy D, et al. 2004. Automatically parcellating the human cerebral cortex. Cerebral Cortex. 14:11–22.
Fjell AM, Sneve MH, Grydeland H, Storsve AB, Amlien IK, Yendiki A, Walhovd KB. 2017. Relationship between structural and functional connectivity change across the adult lifespan: a longitudinal investigation. Hum Brain Mapp. 38: 561–573.
Fransson P, Aden U, Blennow M, Lagercrantz H. 2011. The functional architecture of the infant brain as revealed by resting-state fMRI. Cereb Cortex. 21:145–154.
FreeView. http://surfer.nmr.mgh.harvard.edu/fswiki/FreeviewGuide.
Gao W, Alcauter S, Smith JK, Gilmore JH, Lin W. 2015. Development of human brain cortical network architecture during infancy. Brain Struct Funct. 220:1173–1186.
Gao W, Gilmore JH, Giovanello KS, Smith JK, Shen D, Zhu H, Lin W. 2011. Temporal and spatial evolution of brain network topology during the first two years of life. PLoS One. 6: e25278.
Ghosh A, Antonini A, McConnell SK, Shatz CJ. 1990. Requirement for subplate neurons in the formation of thalamocortical connections. Nature. 347:179–181.
Grayson DS, Ray S, Carpenter S, Iyer S, Dias TG, Stevens C, Nigg JT, Fair DA. 2014. Structural and functional rich club organization of the brain in children and adults. PLoS One. 9: e88297.
Greene DJ, Laumann TO, Dubis JW, Ihnen SK, Neta M, Power JD, Pruett JR Jr., Black KJ, Schlaggar BL. 2014. Developmental changes in the organization of functional connections between the basal ganglia and cerebral cortex. J Neurosci. 34:5842–5854.
Hagmann P, Cammoun L, Gigandet X, Meuli R, Honey CJ, Wedeen VJ, Sporns O. 2008. Mapping the structural core of human cerebral cortex. PLoS Biol. 6:e159.
Honey CJ, Kotter R, Breakspear M, Sporns O. 2007. Network structure of cerebral cortex shapes functional connectivity on multiple time scales. Proc Natl Acad Sci USA. 104: 10240–10245.
Honey CJ, Sporns O, Cammoun L, Gigandet X, Thiran JP, Meuli R, Hagmann P. 2009. Predicting human resting-state functional connectivity from structural connectivity. Proc Natl Acad Sci USA. 106:2035–2040.
Huttenlocher P. 2002. Neural plasticity: the effects of environment on the development of the cerebral cortex. Cambrigde: Harvard University Press.
Huttenlocher PR, Dabholkar AS. 1997. Regional differences in synaptogenesis in human cerebral cortex. J Comp Neurol. 387:167–178.
Huttenlocher PR, de Courten C, Garey LJ, Van der Loos H. 1982. Synaptogenesis in human visual cortex—evidence for synapse elimination during normal development. Neurosci Lett. 33:247–252.
Hwang K, Hallquist MN, Luna B. 2013. The development of hub architecture in the human functional brain network. Cereb Cortex. 23:2380–2393.
Iglesias JE, Sabuncu MR, Van Leemput K 2012. A generative model for multi-atlas segmentation across modalities. Proceedings/IEEE International Symposium on Biomedical Imaging: From Nano to Macro IEEE International Symposium on Biomedical Imaging: pp. 888–891.
Innocenti GM. 1995. Exuberant development of connections, and its possible permissive role in cortical evolution. Trends Neurosci. 18:397–402.
Innocenti GM, Price DJ. 2005. Exuberance in the development of cortical networks. Nat Rev Neurosci. 6:955–965.
Jenkins GM, Watts DG. 1968. Spectral analysis and its applications.. San Francisco: Holden-Day.
Jenkinson M, Bannister P, Brady M, Smith S. 2002. Improved optimization for the robust and accurate linear registration

and motion correction of brain images. Neuroimage. 17: 825–841.

Johansen-Berg H, Behrens TEJ, Sillery E, Ciccarelli O, Thompson AJ, Smith SM, Matthews PM. 2005. Functional–anatomical validation and individual variation of diffusion tractography-based segmentation of the human thalamus. Cereb Cortex. 15:30–39.

Kostovic I, Jovanov-Milosevic N. 2006. The development of cerebral connections during the first 20–45 weeks' gestation. Semin Fetal Neonatal Med. 11:415–422.

Kostovic I, Judas M. 2010. The development of the subplate and thalamocortical connections in the human foetal brain. Acta Paediatr. 99:1119–1127.

Kozberg M, Hillman E. 2016. Neurovascular coupling and energy metabolism in the developing brain. Prog Brain Res. 225: 213–242.

Lagercrantz H, Hanson MA, Ment LR, Peebles DM, editors. 2010. The newborn brain neuroscience and clinical applications. 2nd ed. Cambridge: Cambridge University Press. p. 422. p 1 online resource.

Lam YW, Sherman SM. 2011. Functional organization of the thalamic input to the thalamic reticular nucleus. J Neurosci. 31:6791–6799.

LaMantia AS, Rakic P. 1990. Axon overproduction and elimination in the corpus callosum of the developing rhesus monkey. J Neurosci. 10:2156–2175.

Lokmane L, Proville R, Narboux-Neme N, Gyory I, Keita M, Mailhes C, Lena C, Gaspar P, Grosschedl R, Garel S. 2013. Sensory map transfer to the neocortex relies on pretarget ordering of thalamic axons. Curr Biol. 23:810–816.

Mai JM, Paxinos G, Voss T. 2007. Atlas of the human brain. Academic Press.

Martini FJ, Moreno-Juan V, Filipchuk A, Valdeolmillos M, Lopez-Bendito G. 2018. Impact of thalamocortical input on barrel cortex development. Neuroscience. 368:246–255.

Mastropasqua C, Bozzali M, Spano B, Koch G, Cercignani M. 2015. Functional anatomy of the thalamus as a model of integrated structural and functional connectivity of the human brain in vivo. Brain Topogr. 28:548–558.

McQuillen PS, Ferriero DM. 2005. Perinatal subplate neuron injury: implications for cortical development and plasticity. Brain Pathol. 15:250–260.

Montgomery JM, Madison DV. 2004. Discrete synaptic states define a major mechanism of synapse plasticity. Trends Neurosci. 27:744–750.

Nieuwenhuys R, Voogd J, van Huijzen C. 2008. The human central nervous system—a synopsis and atlas. Heidelberg: Steinkopff-Verlag.

O'Leary DD. 1992. Development of connectional diversity and specificity in the mammalian brain by the pruning of collateral projections. Curr Opin Neurobiol. 2:70–77.

O'Leary DD, Chou SJ, Sahara S. 2007. Area patterning of the mammalian cortex. Neuron. 56:252–269.

Petanjek Z, Judas M, Simic G, Rasin MR, Uylings HB, Rakic P, Kostovic I. 2011. Extraordinary neoteny of synaptic spines in the human prefrontal cortex. Proc Natl Acad Sci USA. 108: 13281–13286.

Poh JS, Li Y, Ratnarajah N, Fortier MV, Chong YS, Kwek K, Saw SM, Gluckman PD, Meaney MJ, Qiu A. 2015. Developmental synchrony of thalamocortical circuits in the neonatal brain. Neuroimage. 116:168–176.

Power JD, Barnes KA, Snyder AZ, Schlaggar BL, Petersen SE. 2012. Spurious but systematic correlations in functional connectivity MRI networks arise from subject motion. Neuroimage. 59: 2142–2154.

Rakic P. 1988. Specification of cerebral cortical areas. Science. 241:170–176.

Rakic P, Riley KP. 1983. Overproduction and elimination of retinal axons in the fetal rhesus monkey. Science. 219:1441–1444.

Ratiu P, Talos I-F. 2006. Cross-sectional atlas of the brain. Cambridge, MA: Harvard University Press.

Reuter M, Schmansky NJ, Rosas HD, Fischl B. 2012. Within-subject template estimation for unbiased longitudinal image analysis. NeuroImage. 61:1402–1418.

Seeley WW, Menon V, Schatzberg AF, Keller J, Glover GH, Kenna H, Reiss AL, Greicius MD. 2007. Dissociable intrinsic connectivity networks for salience processing and executive control. J Neurosci. 27:2349–2356.

Shatz CJ. 1996. Emergence of order in visual system development. J Physiol Paris. 90:141–150.

Skudlarski P, Jagannathan K, Calhoun VD, Hampson M, Skudlarska BA, Pearlson G. 2008. Measuring brain connectivity: diffusion tensor imaging validates resting state temporal correlations. Neuroimage. 43:554–561.

Smith SM, Jenkinson M, Woolrich MW, Beckmann CF, Behrens TE, Johansen-Berg H, Bannister PR, De Luca M, Drobnjak I, Flitney DE, et al. 2004. Advances in functional and structural MR image analysis and implementation as FSL. Neuroimage. 23(Suppl 1):S208–S219.

Smyser CD, Inder TE, Shimony JS, Hill JE, Degnan AJ, Snyder AZ, Neil JJ. 2010. Longitudinal analysis of neural network development in preterm infants. Cereb Cortex. 20:2852–2862.

Smyser CD, Snyder AZ, Neil JJ. 2011. Functional connectivity MRI in infants: exploration of the functional organization of the developing brain. Neuroimage. 56:1437–1452.

Sotiropoulos SN, Jbabdi S, Xu J, Andersson JL, Moeller S, Auerbach EJ, Glasser MF, Hernandez M, Sapiro G, Jenkinson M, et al, Consortium WU-MH. 2013. Advances in diffusion MRI acquisition and processing in the Human Connectome Project. Neuroimage. 80:125–143.

Supekar K, Uddin LQ, Prater K, Amin H, Greicius MD, Menon V. 2010. Development of functional and structural connectivity within the default mode network in young children. Neuroimage. 52:290–301.

Takahashi E, Folkerth RD, Galaburda AM, Grant PE. 2012. Emerging cerebral connectivity in the human fetal brain: an MR tractography study. Cereb Cortex. 22:455–464.

Thomason ME, Grove LE, Lozon TA Jr., Vila AM, Ye Y, Nye MJ, Manning JH, Pappas A, Hernandez-Andrade E, Yeo L, et al. 2015. Age-related increases in long-range connectivity in fetal functional neural connectivity networks in utero. Dev Cogn Neurosci. 11:96–104.

Thompson DK, Chen J, Beare R, Adamson CL, Ellis R, Ahmadzai ZM, Kelly CE, Lee KJ, Zalesky A, Yang JYM, et al. 2016. Structural connectivity relates to perinatal factors and functional impairment at 7years in children born very preterm. Neuroimage. 134:328–337.

Tisdall MD, Hess AT, Reuter M, Meintjes EM, Fischl B, van der Kouwe AJ. 2012. Volumetric navigators for prospective motion correction and selective reacquisition in neuroanatomical MRI. Magn Reson Med. 68:389–399.

Toulmin H, Beckmann CF, O'Muircheartaigh J, Ball G, Nongena P, Makropoulos A, Ederies A, Counsell SJ, Kennea N, Arichi T, et al. 2015. Specialization and integration of functional thalamocortical connectivity in the human infant. Proc Natl Acad Sci USA. 112:6485–6490.

Travis K, Ford K, Jacobs B. 2005. Regional dendritic variation in neonatal human cortex: a quantitative Golgi study. Dev Neurosci. 27:277–287.

Tsang A, Lebel CA, Bray SL, Goodyear BG, Hafeez M, Sotero RC, McCreary CR, Frayne R. 2017. White matter structural connectivity is not correlated to cortical resting-state functional connectivity over the healthy adult lifespan. Front Aging Neurosci. 9:144.

Uddin LQ. 2015. Salience processing and insular cortical function and dysfunction. Nat Rev Neurosci. 16:55–61.

Uylings HBM. 2006. Development of the human cortex and the concept of "critical" or "sensitive" periods. Lang Learn. 56: 59–90.

van der Kouwe AJ, Benner T, Salat DH, Fischl B. 2008. Brain morphometry with multiecho MPRAGE. NeuroImage. 40:559–569.

Vanhatalo S, Lauronen L. 2006. Neonatal SEP—back to bedside with basic science. Semin Fetal Neonatal Med. 11:464–470.

Woolrich MW, Jbabdi S, Patenaude B, Chappell M, Makni S, Behrens T, Beckmann C, Jenkinson M, Smith SM. 2009. Bayesian analysis of neuroimaging data in FSL. NeuroImage. 45:S173–S186.

Xu G, Takahashi E, Folkerth RD, Haynes RL, Volpe JJ, Grant PE, Kinney HC. 2014. Radial coherence of diffusion tractography in the cerebral white matter of the human fetus: neuroanatomic insights. Cereb Cortex. 24:579–592.

Yakovlev PI, Lecours AR. 1967. The myelogenetic cycles of regional maturation in the brain. Oxford: Blackwell.

Zatorre RJ, Fields RD, Johansen-Berg H. 2012. Plasticity in gray and white: neuroimaging changes in brain structure during learning. Nat Neurosci. 15:528–536.

Zhang D, Snyder AZ, Fox MD, Sansbury MW, Shimony JS, Raichle ME. 2008. Intrinsic functional relations between human cerebral cortex and thalamus. J Neurophysiol. 100: 1740–1748.

Zhang D, Snyder AZ, Shimony JS, Fox MD, Raichle ME. 2010. Noninvasive functional and structural connectivity mapping of the human thalamocortical system. Cereb Cortex. 20: 1187–1194.